Cement and Concrete Composites 85 (2018) 92–104

Contents lists available at ScienceDirect

Cement and Concrete Composites

journal homepage: www.elsevier.com/locate/cemconcomp

Pore-scale modeling of chloride ion diffusion in cement microstructures

Yuankai Yang, Moran Wang*

Department of Engineering Mechanics and CNMM, Tsinghua University, Beijing 100084, China

A R T I C L E I N F O

Article history:
Received 12 July 2016
Received in revised form
9 September 2017
Accepted 27 September 2017
Available online 29 September 2017

Keywords:
Chloride ion diffusion
Cement microstructure
Electrokinetic effect
Lattice Boltzmann method

A B S T R A C T

Understanding the mechanism of chloride ion diffusion in cement is significant to improve the reliability of offshore reinforced concrete structures. The chloride ionic diffusivity in cement-based microstructures is predicted by pore-scale modeling using a modified lattice Boltzmann method. Both the Nernst-Planck equation for ion diffusion and the Poisson equation for electrodynamic effect are fully solved. The predicted effective diffusivities in cement-based microstructures with different porosities are in good agreements with the experiment data. The results show that the pore size distribution and Zeta potential of cement-based microstructures directly influence the effective diffusivities of chloride ions. The cement-based microstructure with smaller pore size and higher negative Zeta potential hinders chloride ions corrosion more effectively. The electrokinetic effect on the chloride ionic transport is negligible when the ratio of the maximum-probability pore size and the Debye length is higher than 32 in the cement-based microstructure. For engineering applications, we provide a predictive and easy-to-use formula by up-scaling to correlate the effective chloride ion diffusivity with electrokinetic effect in cement paste.

1. Introduction

Reinforced concrete structures being in the marine environment for a long time, the chloride ions of the seawater are injected into the concrete, causing the corrosion of steel bars [1–4]. The transformation of rusty mild steel is accompanied with the increase of volume inducing the expansion and cracking of concrete, which shortens the service life of reinforced concrete structures [5]. Research on the mechanism of the diffusion of chloride ions in concrete remains a major challenge, but is very significant to improve the reliability of reinforced concrete structure design [6]. The rate of chloride ions ingress depends on numerous conditions including porosity, compactness, hydration, additives and cover thickness [7,8]. Experiments [3] displayed that the steel in normal reinforced concrete did not rust due to a passive film, formed on the surface of steel, for the pH value of pore solution in the concrete over 10. The passive film, an oxide layer thickness of about 10 nm, can suppress the corrosion of iron. The break of the passive film would occur with the pH value lower than 10, leading to the iron dissolution and corrosion. Besides, the chloride ion can reduce the ferric corrosion barrier. Hausmann [9] found the corrosion of steel would not occur until the $[\mathrm{Cl}^-]/[\mathrm{OH}^-] > 0.6$. Therefore it is very crucial to understand the mechanism correctly of ions transport and distribution in porous microstructures.

To experimentally study the ion transport and distribution in concrete at pore scale is expensive and tough, especially when the pore size is very small [10–12]. The measurements may be resulted from multi-factorial coupling and hard to reveal the mechanism. Numerical modeling therefore provides an efficient way to help people know what is happening at pore scale and clarify effects from different factors [13–15]. Liu et al. [16] simulated the steady-state diffusion by the Conjugate Gradient method and solved the distributions of ion concentration in porous cement-based microstructures. Zhang et al. [17] applied the lattice Boltzmann (LB) methods to simulate the ion diffusion in the non-saturated cement paste whose microstructure was generated by HYMOSTRUC3D. The gas-water mixture was established by a modified Shan-Chen multiphase LB model and the diffusion process in the microstructure is solved by another LB model. These recent work opened the door for pore-scale modeling of ion diffusion in concrete, but the electrokinetic effects were ignored which included the ion-ion interaction and the ion-surface interaction. As we know that when an

---

* Corresponding author.
E-mail address: mrwang@tsinghua.edu.cn (M. Wang).

https://doi.org/10.1016/j.cemconcomp.2017.09.014
0958-9465/

electrolyte (even for pure water) meets a solid surface, the surface will be automatically charged because of physical adsorptions and chemical reactions [18,19]. The surface charge will induce an electrical double layer (EDL) near the surface and therefore influence the ion distribution [20]. If the pore size is much larger than the thickness of EDL, the electrokinetic effects on ion diffusion and distribution are negligible; however when the EDL thickness is comparable with the pore size of the cement paste, the electrokinetic effects, including ion-ion interaction and ion-surface interaction, may have a significant impact on ion transport [21–23]. Recently, Monteilhet [24] and Korb [25] have shown through measurements that the microstructures of cement paste mainly consists of nanoscale pores, ranging from 2 to 600 nm. Meanwhile the thickness of EDL is about 200–40 nm when the ionic concentration ranges from 0.05 to 1 mM. Therefore the electrokinetic effects play a key role in ion diffusion and distribution in concrete microstructures and have to be considered in pore-scale modeling.

The aim of this present work is to establish a numerical framework to simulate the diffusion of chloride ions in cement-based microstructures with the electrokinetic effects considered. A modified lattice Poisson Boltzmann model is used to solve the Nernst-Planck equation for ion diffusion and the Poisson equation for electrical potential in the three-dimensional microstructure of cement paste. We are to study the influences from microstructure parameters on macroscopic chloride ion diffusion in cement, to reveal the mechanisms and try to provide useful advices on optimizations of engineering applications by up-scaling analysis.

2. Simulation of cement-based microstructure

In this study, a friendly-used model is proposed to generate the three-dimensional porous complex microstructure of hydration cement paste. The cement particles are dissolved from external to internal during the hydration reaction [26]. With neglecting the chemical details the cement particles surrounded by water can react to produce solid reaction products (surface products) or spontaneously nucleate in the capillary water to products crystals (pore products) [27]. The surface product is mainly calcium silicate hydrate (C-S-H), as well the major pore product is calcium hydroxide (CH). In this model, the method developed by Wang et al. [28] is adopted to generate the initial cement particles and the hydration process is simulated using the algorithm similar to, but not exactly the same as, the microstructural model proposed by Garboczi and Bentz. In our algorithm, we add an extra step, called the “invasion” step. This step ensures the hydration process going on when all remaining cement particles are covered by surface product. Hence, the cement microstructure generated by our model is more consistent with the real cement than that of Garboczi and Bentz. The simulation algorithm is described below.

The QSGS model [28] is adopted to reproduce the cement particles in a 3D domain:

(1) We use the water-cement ratio to calculate the seed distribution probability s_d and stochastically locate the seeds based on the seed distribution probability. The cement particles volume fraction is ϕ_s, hence the water volume fraction is $1-\phi_s$ and the water-cement ratio is expressed as [27]:

$$w/c = \frac{1-\phi_s}{3.2\phi_s}. \tag{1}$$

For 3D simulations, the average cement particles volume is $\pi\overline{d}^3/6$ and $\overline{d}$ is the mean grain size of cement particles. Therefore, the 3D seed distribution probability s_d is:

$$s_d = \frac{\phi_s\delta^3}{\pi\overline{d}^3/6} = \frac{6\delta^3}{\pi\overline{d}^3(3.2w/c+1)}, \tag{2}$$

where δ denotes the lattice constant (grid size).

(2) The seeds grow toward neighboring cells using cellular automata approach.
(3) Repeat step (2) until the fraction of the cement paste approaches ϕ_s.

After the cement particles generated, the procedure of hydration operates by an iteration process and each cycle performs three steps:

(i) The dissolution step: count the number of cells on the surface of cement particles and these cells as the reactive cells extend to the neighboring cells. If growing cells locate in pores, these growing cells are judged to be grown successfully as surface product cells. This step stops until the ratio of the number of growing cells and reactive cement cells reach 1.7. By contrast, pore product cells have 0.61 times the number of reactive cement cells. The pore product cells are randomly distributed in the pore space according to the computing number of pore product cells.
(ii) The diffusion/reaction step: stochastic distributed pore product cells move arbitrarily and stop moving when they contact with other solid cells.
(iii) The invasion step: because the surface product (C-S-H) is still porous media [29–31] where the cations and small neutral molecules can diffuse through and be reactive, the hydration process can continue even when all cement particles are covered by surface product. Yet, since the pores in C-S-H are mostly at nanoscale, and generally its surfaces are negatively charged, the diffusion of negative chloride ions is super slow. In this step, the hydration reactant cells randomly move one step in the location of un-reacted cement cells and then mark as new reactive cement cells and count. When the cement paste reaches the degree of hydration α or is completely hydrated, the cycles quit and cement microstructure is fully formed.

Thus, our model essentially uses three parameters (w/c, α and $\overline{d}$) to control the microstructure of cement. The generated porous cement microstructure is sketched in Fig. 1(a). When the cement solid is set as hyaline, the capillary pore distribution is shown in Fig. 1(b) and the early-age cement pore size distribution shown in Fig. 1(c).

To validate our model on cement microstructure simulation, we generate microstructures with different water-cement ratios and degrees of hydration comparing with the Powers' law [33]. According to the Powers' law, the volume fractions of capillary pores ϕ_{cap} (capillary porosity), and unhydrated cement ϕ_{uc} can be respectively determined as [34]:

$$\phi_{cap} = \frac{w/c-0.36\alpha}{w/c+0.32}, \tag{3}$$

$$\phi_{uc} = \frac{0.32(1-\alpha)}{w/c+0.32}. \tag{4}$$

Fig. 2 indicates that the capillary porosity and the volume fraction of unhydrated cement by our model have good agreements with the empirical results by Eqs. (3) and (4). Therefore, our model is a friendly-use and robust method to generate porous cement microstructures.

3. Mathematical description of ion diffusion in capillary pores

The essence of diffusion is the thermal motion of molecular species in fluids, and the concentration gradient of species is the driving force. In 1970, Collepardi [35] firstly described the chloride ion diffusion in the concrete by the Fick's law with the assumptions of isotropic concrete structure and negligible physical or chemical interactions between ions and cement-based materials:

$$\frac{dC_i}{dt} = \nabla\cdot(D_i \nabla C_i), \tag{5}$$

where C_i, D_i are the concentration and the diffusivity of ions, Na^+ or Cl^-, respectively; and t is the time.

However, the cement-based material is not isotropic and homogenous. Actually, it is a complex heterogeneous composite composed by pores, solid, water, bubbles and so on. Especially, to study the mechanism of chloride ion diffusion in pore scale, the results are not convincing without considering the heterogeneous structures of cement-based materials [36]. The scale we focus on is much larger than the atomistic scale, so that the macroscopic continuous equations are still valid [37,38]. With the electrokinetic effect considered, the mass flux of ions in the pore solution in cement is calculated by Ref. [39]:

$$\boldsymbol{J_i} = -D_i \nabla C_i - e z_i b_i C_i \nabla \psi, \tag{6}$$

where e, z_i and ψ denote the absolute charge of electron, the valance number for ith ion and the local electrical potential. We assume the seawater as the NaCl solution and neglect other ions in this work. Therefore $\boldsymbol{J_i}$ denotes Na^+ and Cl^- species flux, b_i denotes the ion mobility of Na^+ or Cl^-. The ionic flux $\boldsymbol{J_i}$ and the concentration C_i follow continuity equation:

$$\frac{\partial C_i}{\partial t} + \nabla\cdot\boldsymbol{J_i} = 0. \tag{7}$$

Substituting Eq. (6) into Eq. (7) leads to the Nernst-Planck equation.

Since the product of cement hydration is the composition of calcium oxide, silicon oxide and aluminum oxide, the metal oxide surface begins to decompose when in contact with the electrolyte solution (e.g. NaCl solution) and the surface generates silanol groups [18,41]. Therefore, the ions in the electrolyte solution form the EDL near the pore wall because of the electrostatic attraction and ionic thermal motion, as shown in Fig. 3. There is a plane to separate mobile fluid from fluid still adhering to the charged surface, called shear plane. The electric potential on this plane is called Zeta potential (ζ-potential). In the cement-based materials, the surface absorbs positive ions (cations) since the Zeta potential is usually negative. Because of the strong electric attraction near the surface, there is area, called stern layer, where the cations are not movable. The ψ denotes the local electric potential caused by the ionic distribution, which is governed by the Poisson equation [20]:

$$\nabla^2 \psi = -\frac{\rho_e}{\varepsilon_r \varepsilon_0} = -\sum_i \frac{N_A e z C_i}{\varepsilon_r \varepsilon_0}, \tag{8}$$

where ρ_e, N_A and $\varepsilon_r\varepsilon_0$ are the net charge density, the Avogadro's number and the dielectric permittivity of electrolyte solution. For dilute electrolyte solutions, the ionic concentration in the diffuse layer matches with the Boltzmann distribution [42]:

$$C_i = C_{i,\infty} \exp(-e z_i \psi / kT), \tag{9}$$

where $C_{i,\infty}$ denotes the bulk ionic concentration. k and T denote the Boltzmann constant and absolute temperature.

Substituting Eq. (8) into Eq. (9) gives the Poisson-Boltzmann equation [43]:

$$\nabla^2 \psi = -\frac{1}{\varepsilon_r \varepsilon_0} \sum_i N_A e z_i C_{i,\infty} \exp\left(-\frac{e z_i}{kT}\psi\right), \tag{10}$$

which describes the interaction between the electric potential and ionic distribution. Eqs. (6)–(10) govern the electrokinetic ionic transport processes in cement microstructures [44].

The Debye length that characterizes the EDL thickness is defined as:

$$\lambda_D = \sqrt{\frac{\varepsilon_r \varepsilon_0 k T}{2 z_i^2 e^2 N_A C_{i,\infty}}}. \tag{11}$$

It is arduous to determine a suitable boundary condition to depict the electric potential and surface charge distribution at the liquid-solid interface in the porous microstructures [25]. Therefore a constant Zeta potential is still popularly used as the electrical boundary condition: $\psi_{wall} = \zeta$. For the inlet and outlet, we adopt the constant ionic concentration boundaries. At the liquid-solid interfaces, the zero normal flux conditions are applied:

$$\boldsymbol{J_i}\cdot\hat{\boldsymbol{n}} = 0, \tag{12}$$

where the $\hat{\boldsymbol{n}}$ is the unit vector normal to surface.

The macroscopic effective diffusivity D_{eff} in porous media that characterizes the comprehensive ionic transport ability in cement-based materials is defined by:

$$D_{eff} = JL/\Delta C, \tag{13}$$

where J is species flux per unit cross-section in the steady state, L and ΔC are the length and ion concentration difference between inlet and outlet. This effective diffusivity varies with the porosity, geometry, chemical and physical properties of cement-based materials.

4. Lattice Boltzmann method

Lattice Boltzmann method (LBM) is a mesoscopic method based on the molecular motion theory and corresponds to clear physical background. In recent years, LBM has shown amazing performances to analyze fluid flow or heat transfer in porous media with complex geometries [28,44–48]. Benefiting its advantages for modeling transports in porous media, we use LBM to investigate the chloride ions diffusion in cement-based materials in this work. The set of coupled ionic electrodynamic transport governing equations, subjected to the appropriate boundary conditions, are solved by our lattice Boltzmann method codes. The developed codes combine an ion diffusion evolution on discrete lattices to solve the Nernst-Planck equation with an electric potential evolution method on the same set of lattices to solve the nonlinear Poisson equation [49].

4.1. Evolution equation for ion diffusion

We use the following evolution equation to solve the governing equation for ion diffusion of Na^+ or Cl^- [50–52]:

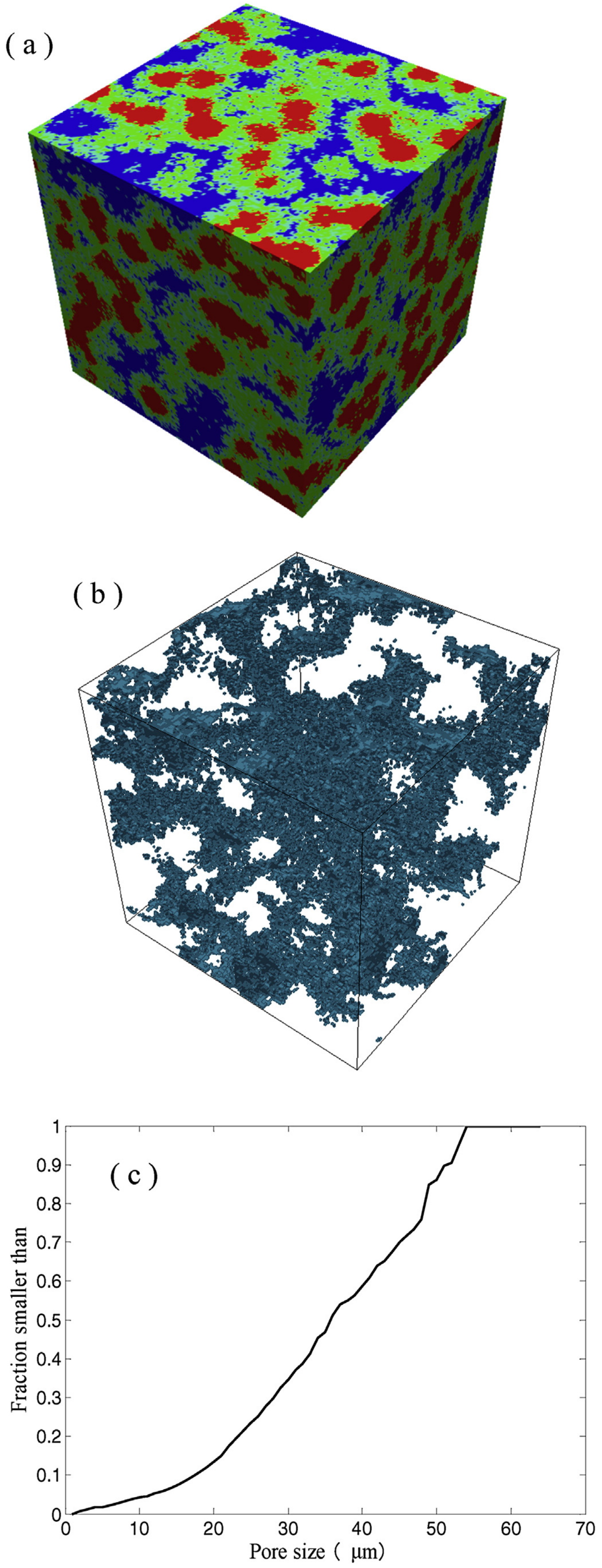

Fig. 1. The three dimension porous microstructure ($140 \times 140 \times 140$ μm^3) of cement generated by our model with a resolution of 2 μm/pixel (a), where the red is the unhydrated cement phase, green is the product of hydration phase and the blue is the capillary pores phase. The capillary pores distribution is shown in (b). The pore size distribution of regenerated early age cement is shown in (c), calculated by the maximum sphere method [32]. (For interpretation of the references to colour in this figure legend, the reader is referred to the web version of this article.)

$$g_\alpha^i(\boldsymbol{r}+\boldsymbol{e}_\alpha\delta_x, t+\delta_{t,D_i}) - g_\alpha^i(\boldsymbol{r},t) = -\frac{1}{\tau_{D_i}}\left[g_\alpha^i(\boldsymbol{r},t) - g_\alpha^{i,eq}(\boldsymbol{r},t)\right], \tag{14}$$

where the $\boldsymbol{r}$ denotes the position vector, $\boldsymbol{e}_\alpha$ the discrete velocities, where $\alpha = 1, 2, \cdots, N$ representing the discretized directions as shown in Fig. 4. The equilibrium distribution function of ionic transport LBM is written as:

$$g_\alpha^{i,eq}(\boldsymbol{r},t) = \left[1 - 4\frac{\delta_{t,D} e z_i D_i}{\delta_x k_B T}\left(\frac{\partial\psi}{\partial x}e_{x,\alpha} + \frac{\partial\psi}{\partial y}e_{y,\alpha} + \frac{\partial\psi}{\partial z}e_{z,\alpha}\right)\right]\omega_\alpha C_i, \tag{15}$$

with

$$\omega_\alpha = \begin{cases} 1/4 & \alpha = 0 \\ 1/8 & \alpha = 1-6 \end{cases}, \tag{16}$$

where τ_{D_i} is the dimensionless relation time for the Na$^+$ or Cl$^-$ ionic transport related to the diffusion coefficient D_i, and δ_{t,D_i} the corresponding time step. The dimensionless relaxation time is calculated by:

$$\tau_{D_i} = \frac{4D_i}{c_{D_i}\delta_x} + \frac{1}{2}, \tag{17}$$

where c_{D_i} is the diffusion lattice speed for Na$^+$ or Cl$^-$ defined as $c_{D_i} = \delta_x/\delta_{t,D_i}$, with δ_x representing the lattice constant (grid size). The value of c_{D_i} can be assigned any positive value as long as the value of $\tau_{D_i} \in (0.5, 2)$ [53]. In the LBM scheme, the macroscopic ionic concentration is calculated by:

$$C_i = \sum_\alpha g_\alpha^i. \tag{18}$$

We choose a consistent D3Q7 scheme for both diffusion and electrical potential evolutions in this work because (i) we tried the D3Q19 scheme for diffusion, but found mass flux oscillations near the boundaries; (ii) the D3Q15 scheme was reported unstable for electrical potential evolution due to the extremely large source term near interfaces [49]. The D3Q7 scheme is stable, accurate enough and highly efficient for diffusion and electrical potential evolutions, compared with the other schemes, even though this scheme is reported not of the same high-order accuracy as D3Q19 for fluid flow. For the D3Q7 lattice system for the evolution equation Eq. (10), the discrete velocities are:

$$\boldsymbol{e}_\alpha = \begin{cases} (0,0,0) & \alpha = 0 \\ (\pm1,0,0), (0,\pm1,0), (0,0,\pm1) & \alpha = 1-6 \end{cases}. \tag{19}$$

4.2. Evolution equation for electrodynamics

The evolution equation for electric potential transport can be therefore written as [50]:

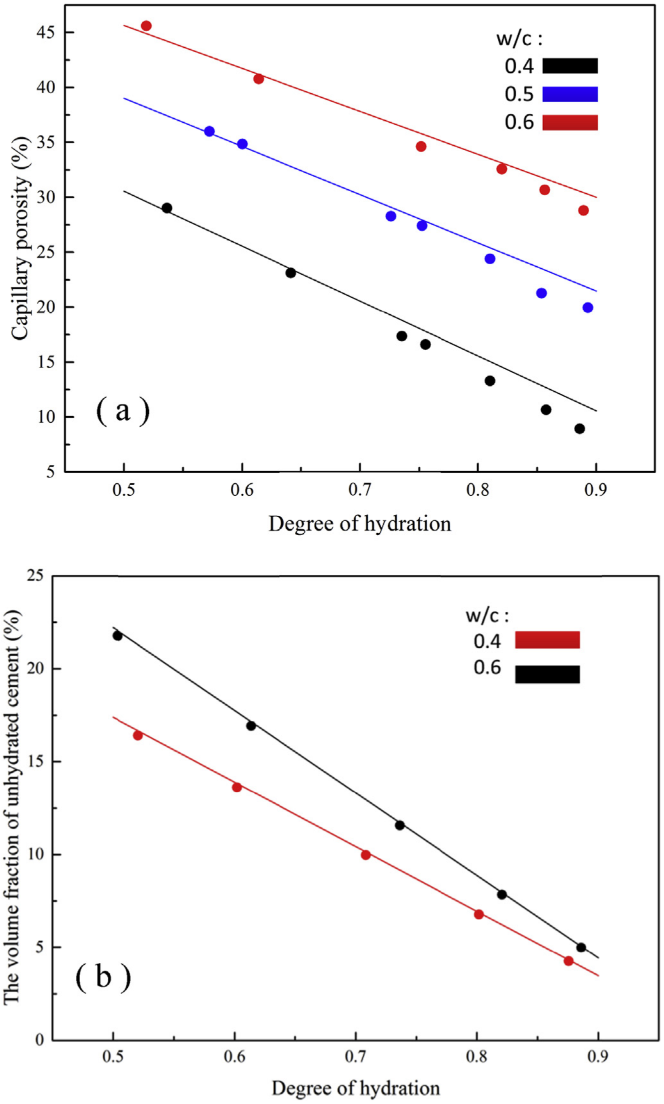

Fig. 2. The capillary porosity and the volume fraction of unhydrated cement varying with the degrees of hydration of present simulations and empirical results are shown in (a) and (b), respectively. Lines represent the empirical results and symbols are from our simulations.

$$h_\alpha\left(\mathbf{r}+\Delta\mathbf{r},t+\delta_{t,\psi}\right)-h_\alpha(\mathbf{r},t)=-\frac{1}{\tau_\psi}\left[h_\alpha(\mathbf{r},t)-h_\alpha^{eq}(\mathbf{r},t)\right]+\omega_\alpha\delta_{t,\psi}\left(1-\frac{0.5}{\tau_\psi}\right)\frac{\rho_e}{\varepsilon_r\varepsilon_0}, \tag{20}$$

where τ_ψ is the dimensionless relaxation time for electric potential transport, c_ψ the electrodynamic lattice speed, which similar to c_{D_i}, defined as $c_\psi=\delta_x/\delta_{t,\psi}$, and $\delta_{t,\psi}$ the time step.

For a D3Q7 lattice system, the equilibrium distribution of electric potential evolution function h_α^{eq} is

$$h_\alpha^{eq}=\begin{cases}0 & \alpha=0\\ \psi/6 & \alpha=1-6\end{cases}, \tag{21}$$

and the dimensionless relaxation time τ_ψ is calculated by:

$$\tau_\psi=\frac{4}{c_\psi\delta_x}+\frac{1}{2}. \tag{22}$$

The macroscopic electrical potential is then calculated by:

$$\psi=\sum_\alpha\left(h_\alpha+0.5\delta_{t,\psi}\omega_\alpha\frac{\rho_e}{\varepsilon_r\varepsilon_0}\right). \tag{23}$$

4.3. Boundary conditions treatments

For ionic transport, the zero normal flux boundary condition translates into [51]:

$$g_\alpha^i\left(\mathbf{r},t+\delta_{t,D_i}\right)=g_\beta^i(\mathbf{r},t), \tag{24}$$

where the index α and β are the opposite directions normal to the interface and β is the direction towards wall. For inlet and outlet boundaries, the Dirichlet boundary condition follows [54]:

$$g_\alpha^i\left(\mathbf{r},t+\delta_{t,D_i}\right)=-g_\beta^i(\mathbf{r},t)+\frac{1}{4}C_0, \tag{25}$$

where C_0 is the given ionic concentration of inlet or outlet.

As for electric potential, we use non-equilibrium “bounce-back” rule as the boundary condition because it is easy to handle for complex geometries [49].

5. Results and discussion

5.1. Benchmark for ions diffusion in channel

To validate our numerical models and codes, firstly we consider ion diffusion in a two-dimensional microchannel, as shown in Fig. 5, with a height H at 0.65 μm. The electrolyte solution is NaCl solution and the initial bulk ionic concentration is 4×10^{-4} mol/L. The inlet and outlet ionic concentrations are given as 5.0×10^{-4} mol/L and 3.0×10^{-4} mol/L, respectively. Meanwhile the other properties and physical parameters are: the diffusivities for both ions $D_{\mathrm{Na^+}}=D_{\mathrm{Cl^-}}=1.5\times10^{-9}$ m^2/s, the dielectric constant $6.95\times10^{-10}\mathrm{C}^2/\mathrm{J{\cdot}m}$ and the temperature 273 K. The surfaces of microchannel are homogeneously charged and the potential distribution should be consistent with that from the Poisson-Boltzmann model for thin electrical double layers from Ref. [55] Chapter 7. The zeta potential for both walls is −20 mV. These parameter ranges are of interest in many civil engineering applications.

Fig. 6(a) shows good agreements between present simulations and theoretical results, which validates the present algorithm and codes. With increase of the distance from the walls, the electrical potential exponentially decays to zero. When the distance is about 4 times of Debye length, the electric potential is less than 3% of zeta potential. Fig. 6(b) illustrates that the concentration gradient of cations along the direction of diffusion near surfaces is much more than the gradient within pores because the cations are converged near the negatively charged walls, and hence the diffusion near surfaces is faster than that in pores.

5.2. Effective ion diffusion coefficient in cement

The actual domain in which we use to simulate the ion diffusion is a 140 × 140 × 140 μm^3 cube with two transition regions shown in Fig. 7. The space discretization depends on the balance between numerical accuracy and computational costs. Since the random

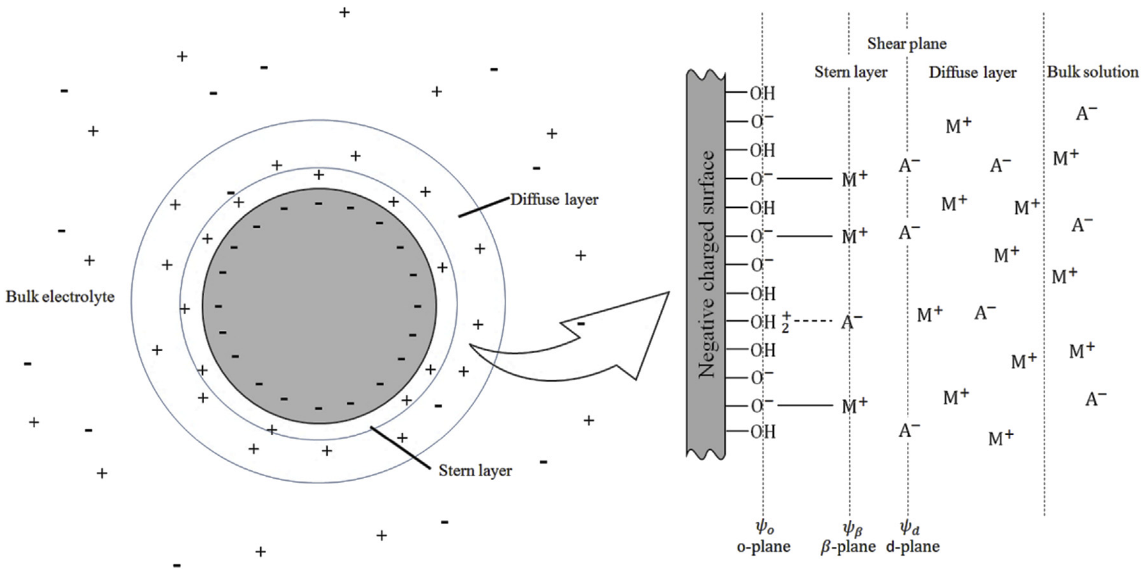

Fig. 3. Sketch of electrical double layer with negative charged surface with the binary monovalent electrolyte [18,40]. M denote the monovalent metal cations (e.g. Na^+, K^+) and A the anions (e.g. Cl^-). The D-plane corresponds here to the shear plane and the Zeta potential, (ζ-potential).

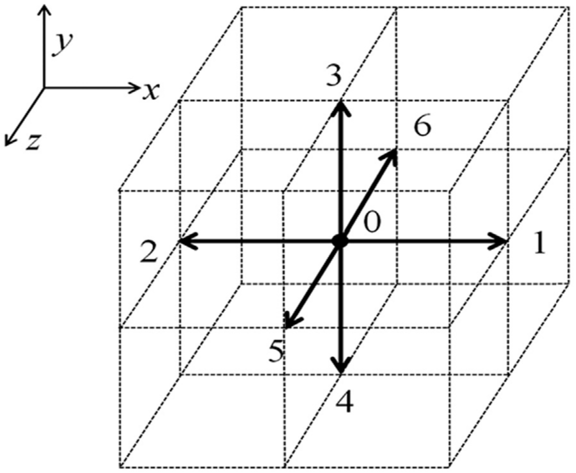

Fig. 4. The discretized directions in D3Q7 model.

characteristics of microstructure leads 3–5% fluctuation in our simulations, a too fine grid is not actually necessary. A 70 × 70 × 70 uniform grid is adopted in our simulations after the grid independence checked. We will also show in the following part of this section that the cube with this set of grid satisfies the REV requirement by our modeling results. We only consider the fully saturated cement in the marine environment in this study. For the degrees of hydration and water to cement ratios studied, the porosities of cement microstructures are all above the percolation threshold, and therefore the chloride ion diffusion process only occurs in the capillary pores while the hydrated phase (e.g. C-S-H) has no contribution to chloride ion diffusion in this work [56,57]. When the porosity is less than percolation threshold, the diffusion process just stops. The bulk diffusivity of chloride ion D_{Cl} in this work is 1.5 × 10^{-9} m^2/s for the room temperature 20 °C from Ref. [58].

We consider a simple binary monovalent electrolyte solution (e.g. NaCl) in the pores. For the absence of electrokinetic effect, the zeta potential for all solid surfaces is set at 0 mV. To investigate the effects of porosity, we compute the effective diffusivities in microstructures with different porosities generated by our model and compare with experimental data. Fig. 8 shows the ionic concentration distributions after the diffusion process is steady. Stochastic characteristics are very clear for the ionic concentration across one section. To calculate the effective ion diffusivity more accurately, we use the arithmetic mean value of one cross-section statistically to eliminate the fluctuations.

Fig. 9 shows the averaged ionic concentration over cross sections varying with position for uncharged or charged porous media under the same ion concentration difference. The effective concentration gradient, defined as $\Delta C/L = (C_i - C_o)/L$, depends on the microstructure and the charge conditions. We use the average concentration at exactly the inlet and the outlet of porous media as C_i and C_o respectively, which have been shown as the intersection points between the red lines (inlet and outlet positions) and the black lines (concentration curve). After the concentration gradient determined, the effective ionic diffusivity is then calculated by Eq. (13) for various microstructures.

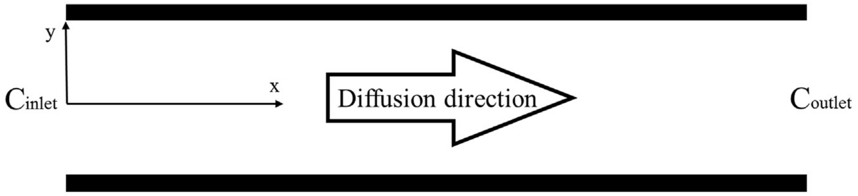

Fig. 5. Ion diffusion in microchannel. The black is the wall. The ionic concentration at inlet and outlet are given.

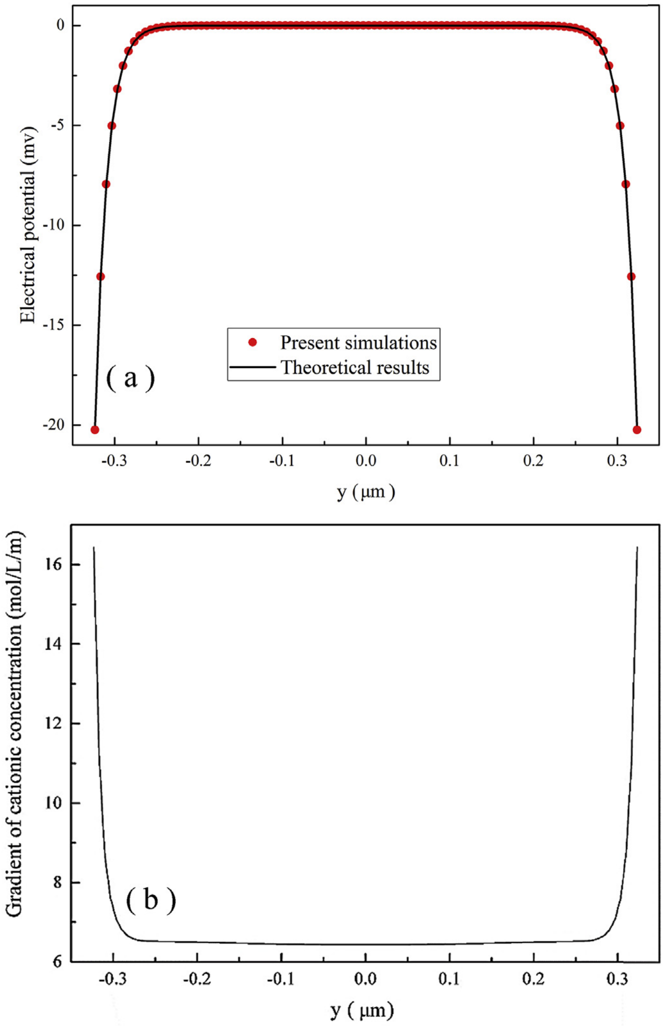

Fig. 6. The electrical potential profile of cross section by the present simulation, compared with the theoretical results, is shown in (a). The theoretical solutions are from Ref. [55]. The Zeta potential is $\zeta = -20$mv. Meanwhile the gradient profile of cationic concentration is shown in (b).

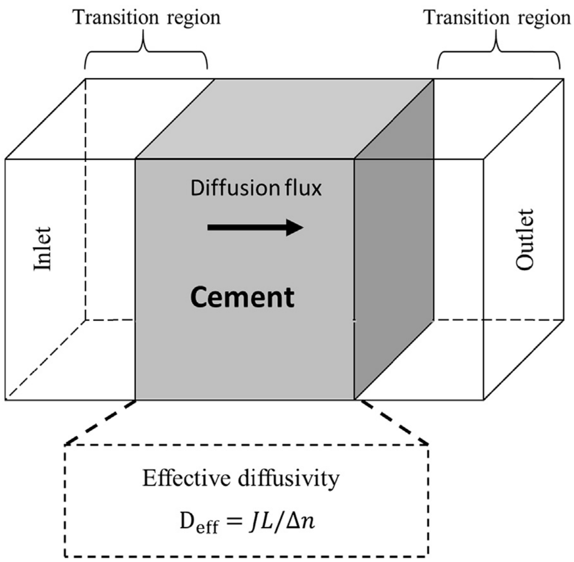

Fig. 7. A sketch about simulation domain.

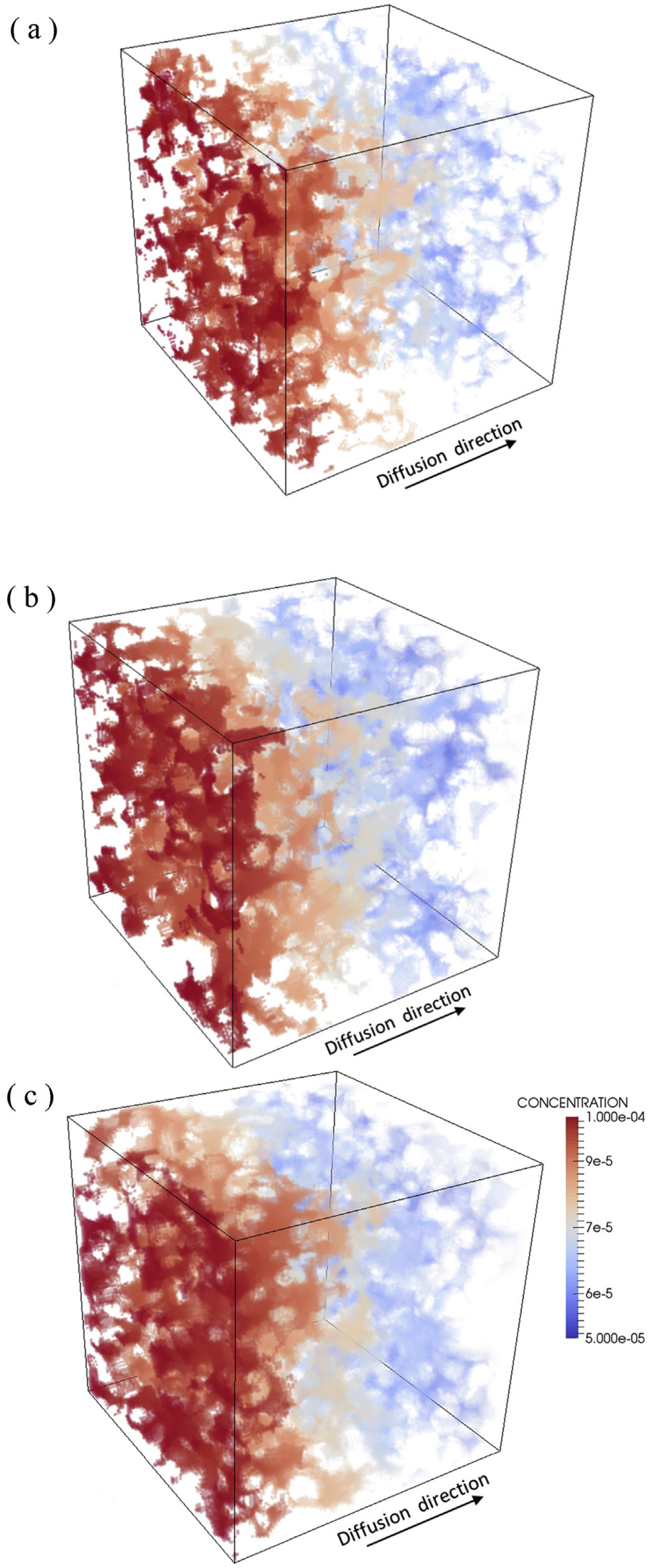

Fig. 8. The distribution of chloride ion concentration in three dimension cement of different porosities when the diffusion is steady. The cement solid is hyaline and invisible. The water-cement ratio: w/c = 0.4 in (a), w/c = 0.5 in (b) and w/c = 0.6 in (c).

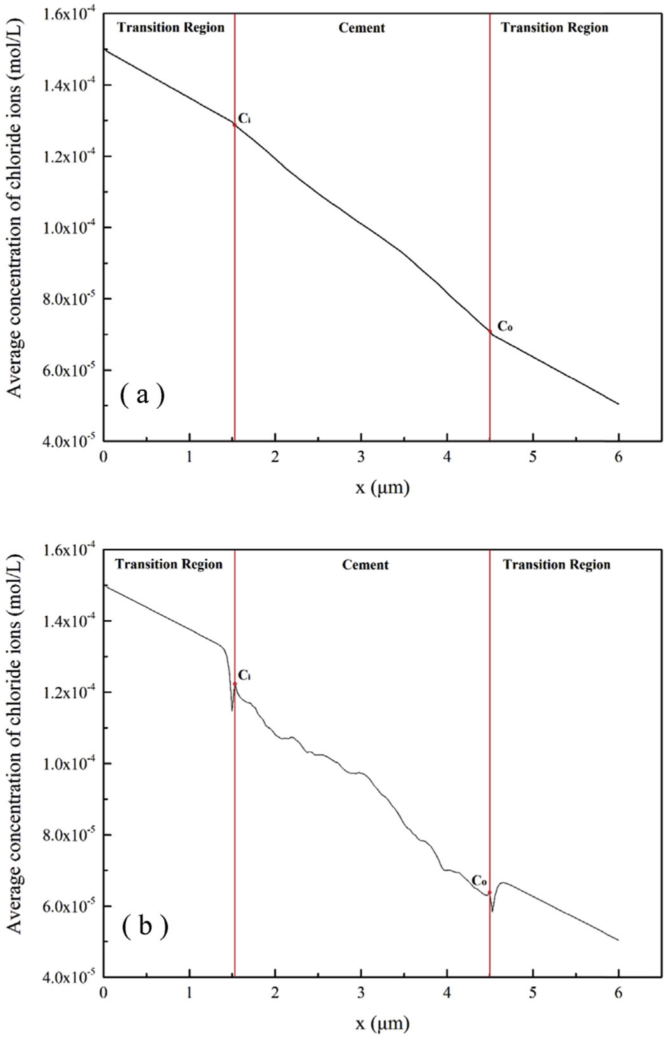

Fig. 9. The schematic mean concentration of each cross section in our simulated domain of cement with uncharged (a) and charged wall (b). The sketch of domain is shown in Fig. 7. The concentration for inlet is 1.5×10^{-4} mol/L and 0.5×10^{-4} mol/L for outlet.

The random factors in generation of microstructures will bring fluctuations to calculation of the effective ion diffusivity. Therefore we have generally generated 3–5 samples for each set of parameters of microstructure and used the mean value as the effective predicted one. For the cube and grid we used mostly, the relative standard deviation of effective diffusivities of the microstructures is 3.6%, less than 5%, which proves this simulated domain can be treated as a REV.

5.3. Chloride ion diffusion without electrokinetic effect

First, simulations are performed in the ordinary Portland cement paste with different porosities. For these cases, we just assign a zero zeta potential to not involve the electrokientic force from solid surfaces. The other physical parameters are the same as the section 5.2. Fig. 10 compares the simulation results with the experimental data reported by others [60–62]. In this study, we ignore the transport process in the gel pores, thus the D_{eff}/D_{Cl} rapidly decreases when the capillary porosity is less than 0.2. From Fig. 10, the effective diffusivity obtained by our simulation is overestimated with respect to experiment data. When we use the modified diffusivity as 1.07×10^{-10} m^2/s suggested by Pivonika et al. [43] to involve the double layer effect, the results show good agreements with experiment data. It means that the electrokinetic effect on ion diffusion in cement is very important and not negligible.

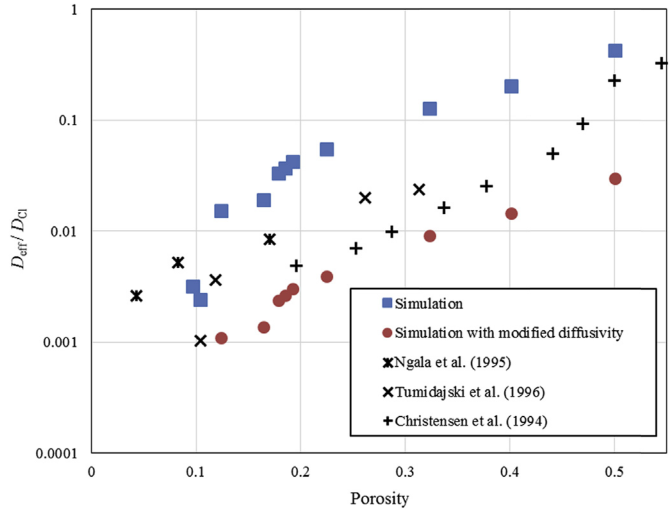

Fig. 10. The comparison of effective chloride diffusivity between simulation and experiment in different porosities. The blue squares are the simulation by using the actual chloride diffusivity and the red circles the simulation with the modified diffusivity as 1.07×10^{-10} m^2/s suggested by Pivonika et al. [58] to consider the double layer effect. (For interpretation of the references to colour in this figure legend, the reader is referred to the web version of this article.)

5.4. Chloride ion diffusion with electrokinetic effect

The electrokinetic effects play an important role on ion diffusion in cement. In this section, we consider the electrokinetic effect and investigate the pore size effect and surface charge statue effect on ion diffusion. To investigate the pore size effect on ionic diffuse ability, here let us characterize the pore size and distinguish some definitions of pore size first: the most probable pore size, the means pore size and the median pore size. The most probable pore size, the maximum probability pore size in pore size distribution, can be recognized as the significant pore size of porous media in pore size distribution [67]. Because the gel pores (smaller than 10 nm) is too weak to affect ionic diffuse ability comparing with mesoscale pores if the capillary porosity is over than 0.2 [56,68], we neglect the gel pores. To study the influence of pore size on the effective diffusivity, a dimensionless number l^*, named the dimensionless pore size, is defined: $l^* = d/\lambda_D$, where d is the characteristic size of pores and λ_D is the Debye length. Therefore after the ionic concentration field is solved out, the significant pore sizes of microstructures are calculated by the scheme proposed by Supriyo and Keith [32].

In this section, we use a computational domain of a $3 \times 3 \times 3$ μm^3 porous microstructure plus two 1.5 μm transition regions with a $200 \times 100 \times 100$ uniform grid, as shown in Fig. 7. For the homogeneous charged surfaces of microstructures, the zeta potential for all walls is −20 mV [69,70]. The chemical composition of pore solution is the symmetric monovalent NaCl electrolyte. The other parameters are the same as stated in the previous section. The distributions of electrical potential and charge density predicted by our numerical frame are shown in Fig. 11.

To quantify the electrokinetic effect on ion diffusion, we compare the calculated effective ion diffusivity by considering or not the wall charges. The effective diffusivity deviation γ is defined as:

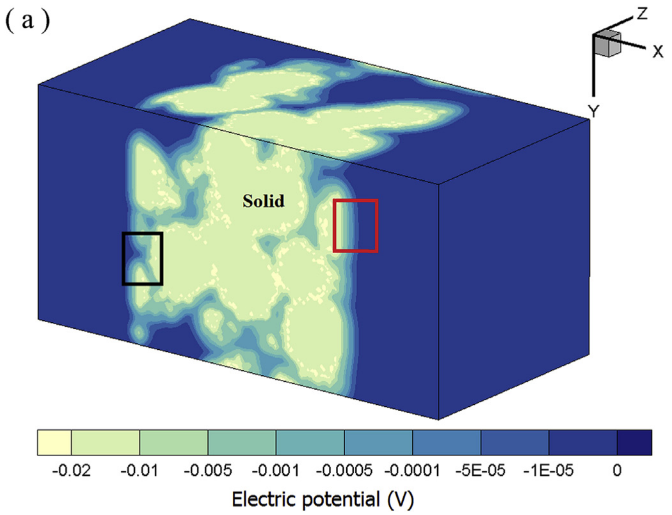

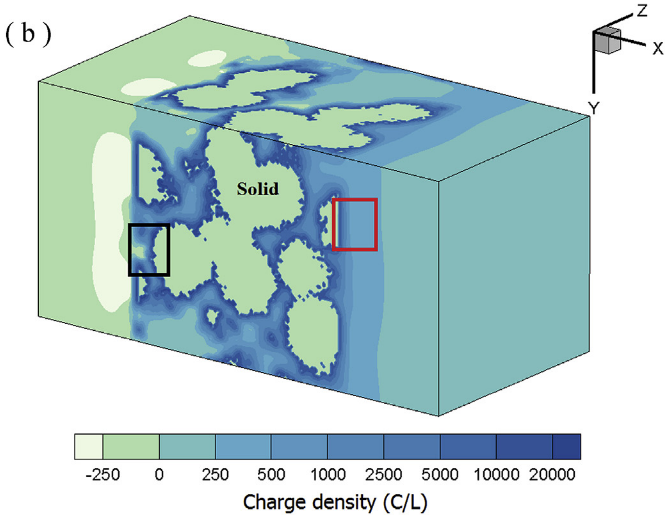

Fig. 11. The distributions of electric potential (a) and charge density (b) presented by our numerical frame. Zeta potential is −20 mV and the direction of diffusion is alone the x axis. Because the bulk concentration in black box is larger than that in red box, the EDL in black box is thinner than that in red box, shown in (a) and (b). (For interpretation of the references to colour in this figure legend, the reader is referred to the web version of this article.)

$$\gamma = \frac{D_{eff} - D^*_{eff}}{D^*_{eff}}, \tag{26}$$

where D_{eff} is the effective diffusivity with electrokinetic effect and D^*_{eff} is that without electrokinetic effect considered of porous microstructures. Fig. 12 shows γ as a function of l^* for different ions. A negative value of deviation denotes that the charged surface can cause the inhibition of ionic transport, while relatively a positive one means the acceleration of ionic diffusion. The results show that the negative zeta potentials can slow down the anionic diffusion and promote the cationic. When l^* increases, the magnitudes of effective diffusivity deviations of both anions and cations decrease. For the anion, the effective diffusivity deviation γ is lower than 10% as $l^* > 32$, which means the electrokinetic effect can be ignored for the anion diffusion provided that $l^* > 32$ in the cement-based microstructure for the civil engineering application.

Fig. 12 also demonstrates that the same l^* exhibits different pore size effects on the anion and cation transport. The pore size effect on the promotion of cations is greater than that on the hindrance of anions. The reason for this is still divergent and may be explained by the details of the surface ionic absorption. The cations are gathered on the solid-liquid interface since the negative charged surface adsorption in the microstructure. Therefore, the concentration gradient of cations along the direction of diffusion near surfaces is much more than the gradient within pores and the cation surface diffusion would be faster than that within pores. As a result, the electrokinetic effect can promote the spread of cations remarkably.

The surface charge status is another important factor for electrokinetic effects on ion diffusion in the porous cement-based microstructure [71]. Fig. 13 shows the calculated effective diffusivities through one single porous microstructure for different Zeta potentials. The results indicate that a higher negative Zeta potential enhances the cationic diffusivity and weakens the anionic. The cation is more sensitive to Zeta potential than the anion. The higher

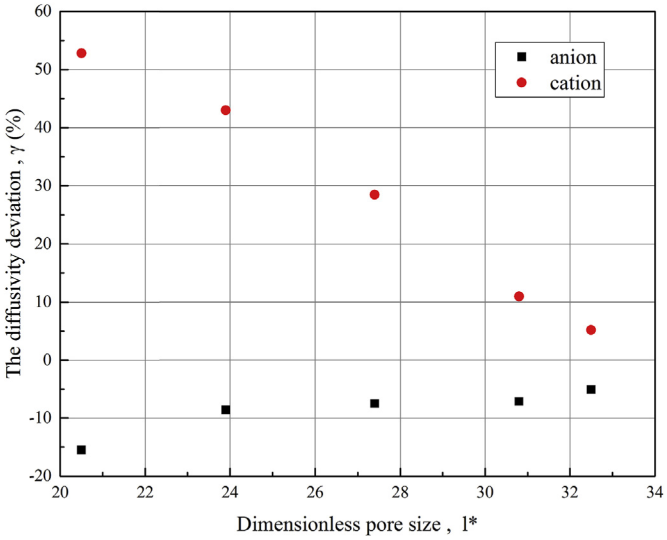

Fig. 12. The deviation of the effective ionic diffusivities with different l^* (Zeta potential = −20 mV).

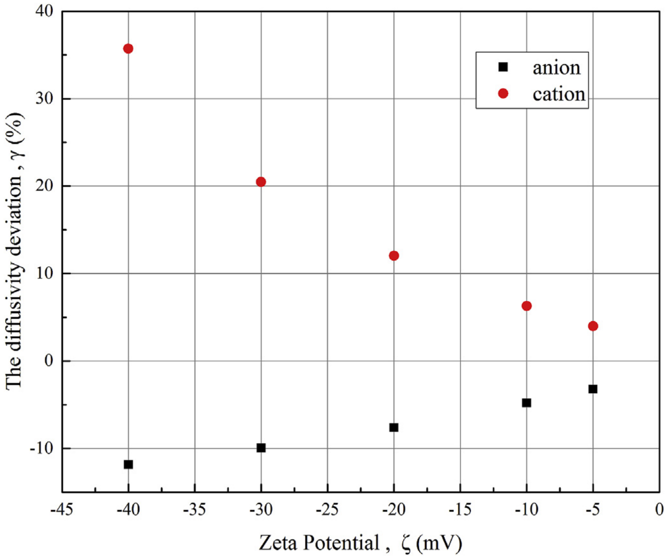

Fig. 13. The deviation of the effective ionic diffusivities with different Zeta potentials ($l^* = 27.4$).

negative Zeta potential forms more intense interaction between ions and the charged surfaces, and leads to higher concentration gradient of cations along the direction of diffusion and therefore a higher effective diffusivity.

6. Predictive formula by up-scaling

So far a powerful numerical framework has been established at pore scale, by which one can reveal the miscroscopic mechanisms of ion transport in cement-based microstructures and even help people correct understanding of the ion diffusion behavior. However this tool is too complicated to use and the process is too time-consuming for engineering application. Therefore we need more friendly-use formulas that can bridge the microstructure details with a macroscopic mathematical expression with parameters. This bridging process is called up-scaling.

Generally the saturated cement paste can be regarded as a two-phase composite, and therefore the effective ionic diffusivity can be expressed as a function of the bulk ionic diffusivity, capillary porosity, tortuosity and constrictivity of pore microstructure, and so on. Based on experimental data, empirical formulas have been proposed for calculating the diffusivity of chloride ions in the cement paste in various situations [64,72]. The fitting parameters in such empirical formulas have to be adapted case by case, which means that they lack generality and physical significance. What is more important is that the previous empirical formulas with fitting parameters can hardly indicate the influences from the microstructure and therefore they are not available for structure design or optimization. However, the process of those empirical formulas inspired us on up-scaling. If one can find a good mathematical expression, and determine the parameters by our pore-scale modeling, one will obtain the predictive formula successfully.

Considering the general effective media theory, the effective species diffusivity in a porous media is following the relationship with pore structure parameters [73]:

$$\frac{D^*_{eff}}{D_0} = \frac{\sigma_{eff}}{\sigma_0} = \phi_{cap}\beta, \tag{27}$$

where D_0 is bulk diffusivity, σ_{eff} and σ_0 is the conductivity through the porous media and the bulk water respectively, ϕ_{cap} denotes the capillary porosity of pore structure, and β is defined as $\beta = \kappa/\tau^2$ [74] with τ representing the tortuosity and κ the constrictivity of the pore structure. τ and κ reflect the complexity of pore network and they are difficult to directly obtain through experiments. Therefore, people have simplified it by using only the capillary porosity, namely the Archie's law, based on the general composite theories, as the pore-network parameter, given as [65]:

$$D^*_{eff} = a\cdot\phi^n_{cap}, \tag{28}$$

where a is a variable relating to D_0 and n is obtained by the constrictivity and tortuosity of the pore network. Arnold et al. [22] introduced specific corrections into Eq. (28) to modified this formula to evaluate effects of other interactions(eg. chemical reactions, electrical potential). The Bruggeman asymmetric medium theory also provided the similar relation to Eqs. (27) and (28), in addition, considering the percolation threshold. To overcome the drawback of the Bruggeman asymmetric medium theory, a more complicated formula was introduced to reveal the chloride ion diffusion in the solid phase of the cement paste, eg. C-S-H gel, which is also diffusive, because of gel pores existed in the C-S-H gel [65].

Near the negative charged surface, the anionic concentration decreases and the cationic concentration increases accordingly in fact. If we still treat the concentration as constant, we can transfer this effect to variations of cross-sectional area for anions. Furthermore, we can even consider charged surfaces change the effective porosity ϕ_{eff} of the cement microstructure for different ions, given as:

$$\phi_{eff} = \omega_e\cdot\phi_{cap}, \tag{29}$$

where ω_e is the correction factor of the electrokinetic effect, written as:

$$\omega_e = \exp\left(-\eta_s b\cdot e^{-\beta_s l^*/2}\right), \tag{30}$$

where η_s and β_s are the correction factors of pores' electrical potential and effective pore radius in the porous media, respectively, b is the dimensionless zeta potential, defined as: $b = z_i e\zeta/k_B T$. For the absence of electrokinetic effect or if $l^* \sim \infty$, $\omega_e = 1$, which means this model is compatible with the previous theoretical models without electrokinetic effects. A full derivation of Eq. (30) is given in the Appendix A. As a result, the effective diffusivity of chloride ions in the cement paste is:

$$D_{eff} = D_0\left(\exp\left(-\eta_s b\cdot e^{-\beta_s l^*/2}\right)\cdot\phi_{cap}\right)^n. \tag{31}$$

Eq. (31) is the proposed predictive mathematical formula that can involve the electrokinetic effects on ion diffusion in porous cement-based materials. There are three parameters that can be determined by fitting the pore-scale modeling results. To observe the electrokinetic effect, we generate six groups of cement-based microstructures, whose mean pore size is comparable with EDL thickness. We use these microstructures as the domains for simulation to calculate the effective diffusivity of chloride ion for different ionic bulk concentrations and zeta potentials. The other parameters are the same as section 5.4. The simulation results shown in Fig. 14 are employed to determine the values of parameters in Eq. (31) by numerical fitting. The results show $n = 1.7$,

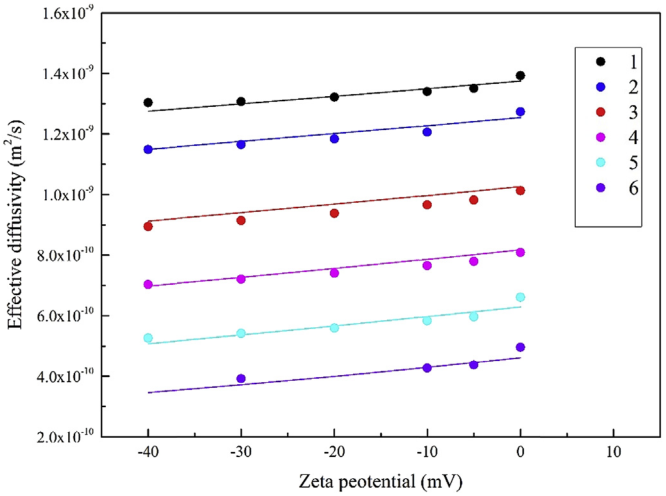

Fig. 14. The comparison between the proposed predictive formula and pore-scale simulations for different Zeta potentials and microstructures. Effective diffusivities vary with the Zeta potentials of different microstructures. The different colors mean various microstructures with corresponding structure. The detailed parameters of each microstructures are: 1, $\phi_{cap} = 0.95$, $l^* = 32.5$; 2, $\phi_{cap} = 0.9$, $l^* = 30.8$; 3, $\phi_{cap} = 0.8$, $l^* = 27.4$; 4, $\phi_{cap} = 0.7$, $l^* = 23.9$; 5, $\phi_{cap} = 0.6$, $l^* = 20.5$; 6, $\phi_{cap} = 0.5$, $l^* = 17.1$. The lines are analytic predictive results by Eq. (32) and symbols are results from numerical simulations. (For interpretation of the references to colour in this figure legend, the reader is referred to the web version of this article.)

$\eta_s = 0.45$, $\beta_s = 0.17$ and we re-write Eq. (31) as:

$$D_{eff} = D_0\left(\exp\left(-0.45b\cdot e^{-0.17l^*/2}\right)\cdot\phi_{cap}\right)^{1.7}. \tag{32}$$

As a result, we predict the effective diffusivity of chloride ion by Eq. (32) for different ionic bulk concentrations. Fig. 15 shows the comparisons between the predicted results and the pore-scale modeling ones. The preview studies [75] also showed the trend that a low solution concentration could weaken the chloride ion effective diffusivity, which is consistent with Eq. (32) qualitatively. Fig. 16 validates the applicability of Eq. (32) in cement with experiment data. Based on the salinity of pore solution in cement, the parameters of Eq. (32) we used are: $\lambda_D = 9.6$ nm, $l^* = 0.83$ and $b = 0,\ 0.79,\ 2.4$ respectively. When the zeta potential is 0 mV, it means that we do not consider the electrical double layer (EDL) effect and again the diffusivity is overestimated by the predictive results without EDL. However, the prediction by Eq. (32) shows a better agreement with experiment data if the EDL effect considered. The good agreements prove the good performance of the proposed predictive formula again.

Even though Eq. (32) is finalized through numerical pore-scale modeling, it may provide predictions of different parameters more quickly, efficiently and deeply. For instance, Fig. 14 tells simply that any negatively charged surface will decrease the diffusivity of negatively charged ion, such as chloride ions; it also tells that the effective ion diffusivity decreases in a super-linear way with the pore size (l^*). Besides, Fig. 14 and Eq. (32) may also deduce strategies to reduce chloride ion corrosion of cement paste: (i) reduce the porosity and enhance the compactness; (ii) decrease the pore size in cement paste as much as possible; (iii) increase the Zeta potential of cement solid surfaces if possible.

7. Conclusions

In this paper, we have established a pore-scale numerical framework to study the ion diffusion with electrokinetic effects in porous microstructures of cements. We developed an algorithm to reconstruct three-dimensional microstructures of saturated cements, whose results agreed well with the Power's law. The transport governing equations were then solved by a high-efficiency coupled LBM code. The numerical results from our pore-scale framework have been validated by comparisons with the available experimental data and theoretical solutions. The present modeling results show that the electrokinetic effect is as a function of the most probable pore size and Zeta potential. The electrokinetic effect on ionic diffusion in the cement declines when the most probable pore size increases and negative Zeta potential decreases. The cationic diffusion is more sensitive to the electrokinetic effect than anionic. If pore size is much larger than the Debye length (i.e. $l^* > 32$) in the cement-based materials, the electrokinetic effect on the chloride ion diffusion is negligible. By upscaling analysis, we proposed a predictive formula for the effective chloride ion diffusivity with electrokinetic effect in porous cement paste. To reduce the chloride ion diffusion and corrosion, engineers can design a cement-based microstructure with the smaller pore size and higher negative Zeta potential as much as possible. The present results may improve the understanding of ionic diffusion in cement microstructure.

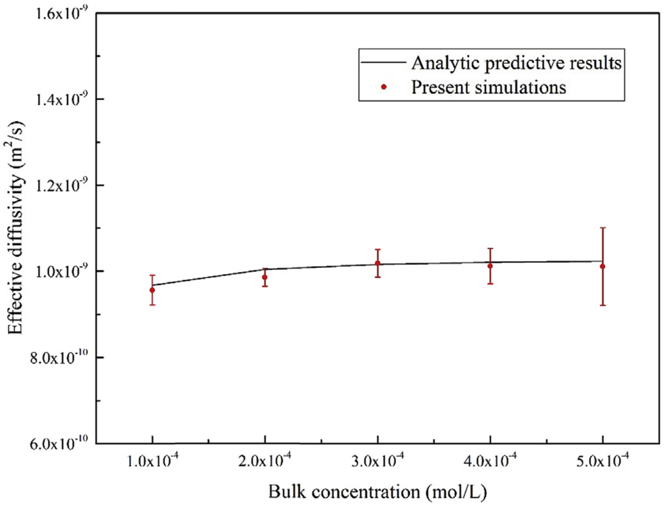

Fig. 15. Relationship between effective diffusivities and bulk concentrations. The lines are analytic predictive results by Eq. (32) and symbols are results from numerical simulations. The Zeta potential is −10 mV and the detailed parameters of cement microstructure is $\phi_{cap} = 0.8$, $l^* = 27.4$.

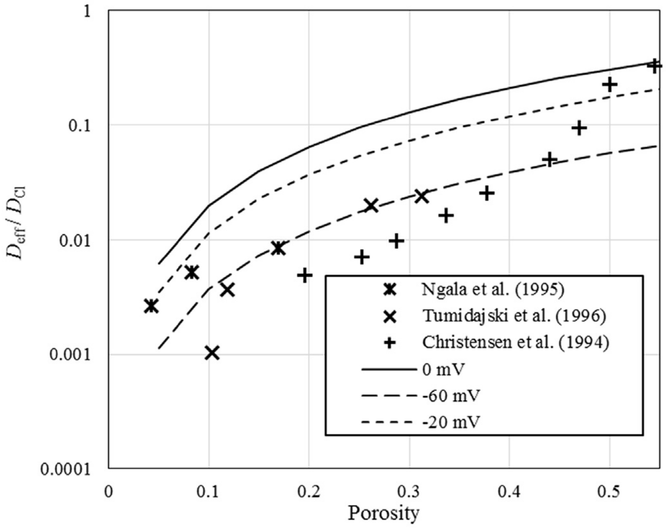

Fig. 16. The comparison of results by Eq. (32) and experiment in different porosities. The lines are analytic predictive results by Eq. (32) and symbols are results from experiment. The Zeta potential for the solid line is zero, which represents the diffusion without electrokinetic effect. The Zeta potential of short dash line is −20 mV and that of long dash line is −60 mV.

Acknowledgements

This work is financially supported by the NSF grant of China (No. 51676107, 51176089) and National Science and Technology Major Project on Oil and Gas (No.2017ZX05013001).

Appendix A

The subsequent formula derivation is based on the following conditions or assumptions: (i) the capillary pores are accepted as equivalent cylinders; (ii) the Debye-Hückel approximation is tenable.

In accordance with Eq. (28), the ionic effective diffusivities in cement paste is given as:

$$D^i_{eff} = D^i_{pore}\phi^n_{eff}, \tag{A.1}$$

where D^i_{pore} is the i ionic effective diffusivity (i is Na$^+$ or Cl$^-$) matching with the sodium chloride diffusivity of a pure solution system. ϕ_{eff} is the effective porosity of the cement microstructure, described as following relationship:

$$\frac{\phi_{eff}}{\phi_{cap}} = \frac{S_{eff}}{S_{cap}}, \tag{A.2}$$

where ϕ_{cap}, S_{cap} is the true capillary porosity and cross-sectional area. S_{eff} is the effective cross-sectional area of capillary pores available for ionic diffusion. For the computing of the effective cross-sectional, we postulate total concentration of the cross-section in the charged cylindrical capillary pores is equal to that in the uncharged capillary pores, whose cross-section is the effective cross-section for ionic diffusion, regressed as:

$$C^i_{total} = \iint_{S_{cap}} r \cdot C_i(r) dr d\theta = \iint_{S_{eff}} C_{i,\infty} ds, \tag{A.3}$$

where C^i_{total} is the total concentration of the cross-section and $C_i(r)$ satisfies the Boltzmann distribution:

$$C_i(r) = C_{i,\infty} \exp\left[-\eta_s \frac{ez_i\psi(r)}{k_B T}\right], \tag{A.4}$$

where η_s is the pores' electrical potential correction factor in porous media. Based on the Debye-Hückel approximation, $\psi(r)$ is roughly written as [76]:

$$\psi(r) = \zeta e^{-(\beta_s R - r)/\lambda_D}, \tag{A.5}$$

where β_s is correction factor of effective pores' radius in the porous media. Summing Eqs. (A.4) and (A.5) with (A.3) results in:

$$2\pi \int_0^{\beta_s R = d/2} r \cdot C_{i,\infty} \exp\left[-\eta_s \frac{ez_i\zeta}{k_B T} e^{-(R-r)/\lambda_D}\right] dr = S_{eff} C_{i,\infty}. \tag{A.6}$$

The left integration term is extremely challenging to get the analytic solution. Hence, the Taylor expansion of the term at zero within the integration on the left-hand side of Eq. (A.6) is performed as follows, taking to the second order

$$r \cdot \exp\left[-\eta_s \frac{ez_i\zeta}{k_B T} e^{-(\beta_s R - r)/\lambda_D}\right] \simeq e^{-\eta_s b \exp(-\beta_s R/\lambda_D)} \cdot r - \frac{\eta_s b}{\lambda_D} e^{-\eta_s b \exp(-\beta_s R/\lambda_D) - \beta_s R/\lambda_D} \cdot r^2. \tag{A.7}$$

Substituting Eq. (A.7) into Eq. (A.6) and integrating gives:

$$S_{eff} \Big/ S_{cap} = S_{eff} \Big/ \left(\pi(\beta_s R)^2\right) = e^{-\eta_s b \cdot e^{-\beta_s l^*/2}} \left(1 - \frac{2}{3}\eta_s b \beta_s l^* e^{-\beta_s l^*/2}\right), \tag{A.8}$$

where l^* is the dimensionless pore size. For $l^* > 10$, $l^* \exp(-l^*/2) \ll 1$, and Eq. (A.8) can be simplified as:

$$S_{eff} \Big/ S_{cap} = e^{-\eta_s b \cdot \exp(-\beta_s l^*/2)}. \tag{A.9}$$

Therefore, the effective porosity of the cement microstructure with the charged surface is:

$$\phi_{eff} = \frac{S_{eff}}{S_{cap}} \phi_{cap} = \exp\left(-\eta_s b \cdot e^{-\beta_s l^*/2}\right) \phi_{cap}, \tag{A.10}$$

then cast Eq. (28) in term of the correction factor:

$$D_{eff} = D_0 \left(\omega_e \cdot \phi_{cap}\right)^n, \tag{A.11}$$

$$\omega_e = \exp\left(-\eta_s b \cdot e^{-\beta_s l^*/2}\right), \tag{A.12}$$

References

[1] C. Obrecht, F. Kuznik, B. Tourancheau, J.-J. Roux, A new approach to the lattice Boltzmann method for graphics processing units, Comput. Math. Appl. 61 (12) (2011) 3628–3638.

[2] M. Manera, O. Vennesland, L. Bertolini, Chloride threshold for rebar corrosion in concrete with addition of silica fume, Corros. Sci. 50 (2) (2008) 554–560.

[3] B. Huet, V. L'Hostis, F. Miserque, H. Idrissi, Electrochemical behavior of mild steel in concrete: influence of pH and carbonate content of concrete pore solution, Electrochim Acta 51 (1) (2005) 172–180.

[4] M. Thomas, Chloride thresholds in marine concrete, Cem. Concr. Res. 26 (4) (1996) 513–519.

[5] C.B. Shin, E.K. Kim, Modeling of chloride ion ingress in coastal concrete, Cem. Concr. Res. 32 (5) (2002) 757–762.

[6] J. Perko, R.A. Patel, Single-relaxation-time lattice Boltzmann scheme for advection-diffusion problems with large diffusion-coefficient heterogeneities and high-advection transport, Phys. Rev. E 89 (5) (2014) 053309.

[7] D.P.G.E.J. Bentz, E.S. Lagergren, Multi-scale microstructural modelling of concrete diffusivity: identification of significant variables, Cem. Concr. Aggregates 20 (1) (1998) 129–139.

[8] A. Boddy, E. Bentz, M.D.A. Thomas, R.D. Hooton, An overview and sensitivity study of a multimechanistic chloride transport model, Cem. Concr. Res. 29 (6) (1999) 827–837.

[9] D. Hausmann, Steel corrosion in concrete—How does it occur? Mater. Prot. 6 (11) (1967) 19–23.

[10] D.P. Bentz, O.M. Jensen, A.M. Coats, F.P. Glasser, Influence of silica fume on diffusivity in cement-based materials: I. Experimental and computer modeling studies on cement pastes, Cem. Concr. Res. 30 (6) (2000) 953–962.

[11] H. Friedmann, O. Amiri, A. Aït-Mokhtar, P. Dumargue, A direct method for determining chloride diffusion coefficient by using migration test, Cem. Concr. Res. 34 (11) (2004) 1967–1973.

[12] K. Krabbenhøft, J. Krabbenhøft, Application of the poisson—nernst—planck equations to the migration test, Cem. Concr. Res. 38 (1) (2008) 77–88.

[13] D.P. Bentz, E.J. Garboczi, Modelling the leaching of calcium hydroxide from cement paste: effects on pore space percolation and diffusivity, Mater Struct. 25 (9) (1992) 523–533.

[14] M.Z. Zhang, G. Ye, K. van Breugel, A numerical-statistical approach to determining the representative elementary volume (REV) of cement paste for measuring diffusivity, Mater. Construcción 60 (300) (2010) 14.

[15] N. Ukrainczyk, E.A.B. Koenders, Representative elementary volumes for 3D modeling of mass transport in cementitious materials, Modell. Simul. Mater Sci. Eng. 22 (3) (2014) 035001.

[16] L. Liu, H. Chen, W. Sun, G. Ye, Microstructure-based modeling of the diffusivity of cement paste with micro-cracks, Constr. Build. Mater. 38 (0) (2013) 1107–1116.

[17] M. Zhang, G. Ye, K. van Breugel, Modeling of ionic diffusivity in non-saturated cement-based materials using lattice Boltzmann method, Cem. Concr. Res. 42 (11) (2012) 1524–1533.

[18] A. Revil, P. Leroy, Constitutive equations for ionic transport in porous shales, J. Geophys. Res. Solid Earth (1978–2012) 109 (B3) (2004) 208.

[19] B. Johannesson, Development of a generalized version of the Poisson—nernst—planck equations using the hybrid mixture theory: presentation of 2D numerical examples, Transp. Porous Media 85 (2) (2010) 565–592.

[20] D. Li, Electrokinetics in Microfluidics, Academic, Oxford, 2004.

[21] P.T. Nguyen, O. Amiri, Study of electrical double layer effect on chloride transport in unsaturated concrete, Constr. Build. Mater. 50 (0) (2014) 492–498.

[22] J. Arnold, D.S. Kosson, A. Garrabrants, J.C.L. Meeussen, H.A. van der Sloot, Solution of the nonlinear Poisson—Boltzmann equation: application to ionic diffusion in cementitious materials, Cem. Concr. Res. 44 (2013) 8–17.

[23] S. Chatterji, Colloid electrochemistry of saturated cement paste and some properties of cement based materials, Adv. Cem. Based Mater. 7 (3–4) (1998) 102–108.

[24] L. Monteilhet, J.P. Korb, J. Mitchell, P.J. McDonald, Observation of exchange of micropore water in cement pastes by two-dimensional T2 -T2 nuclear magnetic resonance relaxometry, Phys. Rev. E 74 (6) (2006) 061404.

[25] J.P. Korb, L. Monteilhet, P.J. McDonald, J. Mitchell, Microstructure and texture of hydrated cement-based materials: a proton field cycling relaxometry approach, Cem. Concr. Res. 37 (3) (2007) 295–302.

[26] C. Huber, B. Chopard, M. Manga, A lattice Boltzmann model for coupled diffusion, J. Comput. Phys. 229 (20) (2010) 7956–7976.

[27] E.J. Garboczi, D.P. Bentz, Computer simulation of the diffusivity of cement-based materials, J. Mater. Sci. 27 (8) (1992) 2083–2092.

[28] M. Wang, J. Wang, N. Pan, S. Chen, Mesoscopic predictions of the effective thermal conductivity for microscale random porous media, Phys. Rev. E 75 (3)

(2007) 036702.

[29] R.F. Feldman, The flow of helium into the interlayer spaces of hydrated portland cement paste, Cem. Concr. Res. 1 (3) (1971) 285–300.

[30] C.K. Yip, J.S.J. van Deventer, Microanalysis of calcium silicate hydrate gel formed within a geopolymeric binder, J. Mater. Sci. 38 (18) (2003) 3851–3860.

[31] H. Li, E. Fratini, W.-S. Chiang, P. Baglioni, E. Mamontov, S.-H. Chen, Dynamic behavior of hydration water in calcium-silicate-hydrate gel: a quasielastic neutron scattering spectroscopy investigation, Phys. Rev. E 86 (6) (2012) 061505.

[32] S. Bhattacharya, K.E. Gubbins, Fast method for computing pore size distributions of model materials, Langmuir 22 (18) (2006) 7726–7731.

[33] T.C. Powers, T.L. Brownyard, Studies of the physical properties of hardened portland cement paste, J. Proc. 43 (9) (1946) 249–336.

[34] T.C. Hansen, Physical structure of hardened cement paste. A classical approach, Mater Struct. 19 (6) (1986) 423–436.

[35] M. Collepardi, A. Marcialis, R. Turriziani, Penetration of chloride ions into cement pastes and concretes, J. Am. Ceram. Soc. 55 (10) (1972) 534–535.

[36] P. Adler, Porous Media: Geometry and Transports, Elsevier, 1992.

[37] J. Wang, M. Wang, Z. Li, Lattice Poisson–Boltzmann simulations of electro-osmotic flows in microchannels, J. Colloid Interface Sci. 296 (2) (2006) 729–736.

[38] M. Wang, S.Y. Chen, On applicability of Poisson-Boltzmann equation for micro- and nanoscale electroosmotic flows, Commun. Comput. Phys. 3 (5) (2008) 1087–1099.

[39] VGe Levich, C.W. Tobias, Physicochemical hydrodynamics, J. Electrochem Soc. 110 (11) (1963), 251C–2C.

[40] P. Leroy, A. Revil, A triple-layer model of the surface electrochemical properties of clay minerals, J. Colloid Interface Sci. 270 (2) (2004) 371–380.

[41] R.K. Iler, The chemistry of silica: solubility, polymerization, colloid and surface pro perties, and biochemistry, Wiley, 1979.

[42] M. Wang, S. Chen, On applicability of Poisson–Boltzmann equation for micro- and nanoscale electroosmotic flows, Commun. Comput. Phys. 3 (5) (2008) 1087–1099.

[43] M. Wang, Structure effects on electro-osmosis in microporous media, J. Heat. Transf. 134 (5) (2012) 051020.

[44] M. Wang, S. Chen, Electroosmosis in homogeneously charged micro- and nanoscale random porous media, J. Colloid Interface Sci. 314 (1) (2007) 264–273.

[45] M. Wang, N. Pan, Predictions of effective physical properties of complex multiphase materials, Mater. Sci. Eng. R Rep. 63 (1) (2008) 1–30.

[46] Q-f Liu, L-y Li, D. Easterbrook, J. Yang, Multi-phase modelling of ionic transport in concrete when subjected to an externally applied electric field, Eng. Struct. 42 (2012) 201–213.

[47] M. Zalzale, P.J. McDonald, Lattice Boltzmann simulations of the permeability and capillary adsorption of cement model microstructures, Cem. Concr. Res. 42 (12) (2012) 1601–1610.

[48] M. Zalzale, P.J. McDonald, K.L. Scrivener, A 3D lattice Boltzmann effective media study: understanding the role of C-S-H and water saturation on the permeability of cement paste, Modell. Simul. Mater Sci. Eng. 21 (8) (2013) 085016.

[49] M. Wang, Q. Kang, Electrokinetic transport in microchannels with random roughness, Anal. Chem. 81 (8) (2009) 2953–2961.

[50] M. Wang, Q. Kang, Modeling electrokinetic flows in microchannels using coupled lattice Boltzmann methods, J. Comput. Phys. 229 (3) (2010) 728–744.

[51] H. Yoshida, T. Kinjo, H. Washizu, Coupled lattice Boltzmann method for simulating electrokinetic flows: a localized scheme for the Nernst–Plank model, Commun. Nonlinear Sci. Numer. Simul. 19 (10) (2014) 3570–3590.

[52] E.G. Flekkøy, Lattice Bhatnagar-Gross-Krook models for miscible fluids, Phys. Rev. E 47 (6) (1993) 4247–4257.

[53] J. Wang, M. Wang, Z. Li, Lattice evolution solution for the nonlinear Poisson–Boltzmann equation in confined domains, Commun. Nonlinear Sci. Numer. Simul. 13 (3) (2008) 575–583.

[54] H. Yoshida, M. Nagaoka, Multiple-relaxation-time lattice Boltzmann model for the convection and anisotropic diffusion equation, J. Comput. Phys. 229 (20) (2010) 7774–7795.

[55] J.S. Duncan, Introduction to Colloid and Surface Chemistry, Elsevier Science Ltd, 1992.

[56] E.J. Garboczi, D.P. Bentz, The effect of statistical fluctuation, finite size error, and digital resolution on the phase percolation and transport properties of the NIST cement hydration model, Cem. Concr. Res. 31 (10) (2001) 1501–1514.

[57] D.P. Bentz, E.J. Garboczi, Percolation of phases in a three-dimensional cement paste microstructural model, Cem. Concr. Res. 21 (2) (1991) 325–344.

[58] P. Pivonka, C. Hellmich, D. Smith, Microscopic effects on chloride diffusivity of cement pastes—a scale-transition analysis, Cem. Concr. Res. 34 (12) (2004) 2251–2260.

[60] V.T. Ngala, C.L. Page, L.J. Parrott, S.W. Yu, Diffusion in cementitious materials: II, further investigations of chloride and oxygen diffusion in well-cured OPC and OPC/30%PFA pastes, Cem. Concr. Res. 25 (4) (1995) 819–826.

[61] P.J. Tumidajski, A.S. Schumacher, S. Perron, P. Gu, J.J. Beaudoin, On the relationship between porosity and electrical resistivity in cementitious systems, Cem. Concr. Res. 26 (4) (1996) 539–544.

[62] K.D. Stanish, R.D. Hooton, M.D.A. Thomas, Testing the Chloride Penetration Resistance of Concrete: a Literature Review. FHWA Contract DTFH61-97-R-00022 “Prediction of Chloride Penetration in Concrete”, Department of Civil Engineering, University of Toronto, Canada, 1997.

[64] D.P. Bentz, A virtual rapid chloride permeability test, Cem. Concr. Compos 29 (10) (2007) 723–731.

[65] B.H. Oh, S.Y. Jang, Prediction of diffusivity of concrete based on simple analytic equations, Cem. Concr. Res. 34 (3) (2004) 463–480.

[67] M. Schmidt, E. Fehling, Ultra-high-performance concrete: research, development and application in Europe, ACI Spec. Publ. 228 (2005) 51–78.

[68] E. Gallucci, K. Scrivener, A. Groso, M. Stampanoni, G. Margaritondo, 3D experimental investigation of the microstructure of cement pastes using synchrotron X-ray microtomography (μCT), Cem. Concr. Res. 37 (3) (2007) 360–368.

[69] S. Chatterji, M. Kawamura, Electrical double layer, ion transport and reactions in hardened cement paste, Cem. Concr. Res. 22 (5) (1992) 774–782.

[70] K. Popov, I. Glazkova, S. Myagkov, A. Petrov, E. Sedykh, L. Bannykh, et al., Zeta-potential of concrete in presence of chelating agents, Colloids Surf. Physicochem Eng. Asp. 299 (1–3) (2007) 198–202.

[71] M.M. Jensen, A Coupled Transport and Chem-ical Model for Durability Predictions of Cement Based Ma-terials, Technical University of Denmark, 2014.

[72] X.-Y. Wang, H.-S. Lee, Modeling of chloride diffusion in concrete containing low-calcium fly ash, Mater Chem. Phys. 138 (2–3) (2013) 917–928.

[73] E.J. Garboczi, Permeability, diffusivity, and microstructural parameters: a critical review, Cem. Concr. Res. 20 (4) (1990) 591–601.

[74] J. van Brakel, P.M. Heertjes, Analysis of diffusion in macroporous media in terms of a porosity, a tortuosity and a constrictivity factor, Int. J. Heat. Mass Transf. 17 (9) (1974) 1093–1103.

[75] S. Chatterji, Transportation of ions through cement based materials. Part 3 experimental evidence for the basic equations and some important deductions, Cem. Concr. Res. 24 (7) (1994) 1229–1236.

[76] R.F. Probstein, Physicochemical Hydrodynamics: an Introduction, John Wiley & Sons, 2005.